

JGR Biogeosciences

RESEARCH ARTICLE

10.1029/2019JG005029

Key Points:

- We disentangle chlorophyll fluorescence spectra into three distinct components explaining >95% of the variance in the spectral shape
- The spectral shape of chlorophyll fluorescence is stable >740 nm, modulated by distinct chlorophyll and nonphotochemical quenching features
- Using spectral shape changes to infer plant stress via remote sensing will be challenging—mostly dominated by chlorophyll and structure

Supporting Information:

- Supporting Information S1

Correspondence to:

T. S. Magney,
tmagney@caltech.edu

Citation:

Magney, T. S., Frankenberg, C., Köhler, P., North, G., Davis, T. S., Dold, C., et al. (2019). Disentangling changes in the spectral shape of chlorophyll fluorescence: Implications for remote sensing of photosynthesis. *Journal of Geophysical Research: Biogeosciences*, 124, 1491–1507. <https://doi.org/10.1029/2019JG005029>

Received 14 JAN 2019

Accepted 26 APR 2019

Accepted article online 7 MAY 2019

Published online 20 JUN 2019

Author Contributions:

Conceptualization: Troy S. Magney, Christian Frankenberg, Albert Porcar-Castell

Data curation: Troy S. Magney, Christian Dold







Formal analysis: Troy S. Magney, Christian Frankenberg, Christian Dold, Debsunder Dutta, Alexis Harrington

Funding acquisition: Troy S. Magney, Christian Frankenberg, Jerry Hatfield, Jochen Stutz

Investigation: Troy S. Magney, Christian Frankenberg, Gretchen North, Thomas S. Davis, Christian Dold, Debsunder Dutta, Joshua B. Fisher, Katja Grossmann, Alexis
(continued)

©2019. American Geophysical Union.
All Rights Reserved.

Disentangling Changes in the Spectral Shape of Chlorophyll Fluorescence: Implications for Remote Sensing of Photosynthesis

Troy S. Magney^{1,2} , Christian Frankenberg^{1,2}, Philipp Köhler¹ , Gretchen North³, Thomas S. Davis⁴, Christian Dold⁵, Debsunder Dutta^{1,2} , Joshua B. Fisher², Katja Grossmann⁶, Alexis Harrington³, Jerry Hatfield⁵, Jochen Stutz⁶ , Ying Sun⁷ , and Albert Porcar-Castell⁸ 

¹Division of Geological and Planetary Sciences, California Institute of Technology, Pasadena, CA, USA, ²Jet Propulsion Laboratory, California Institute of Technology, Pasadena, CA, USA, ³Department of Biology, Occidental College, Los Angeles, CA, USA, ⁴Forest and Rangeland Stewardship, Colorado State University, Fort Collins, CO, USA, ⁵National Laboratory for Agriculture and the Environment, USDA-ARS, Ames, IA, USA, ⁶Department of Atmospheric and Oceanic Sciences, University of California, Los Angeles, CA, USA, ⁷Soil and Crop Sciences Section, School of Integrative Plant Science, Cornell University, Ithaca, NY, USA, ⁸Optics of Photosynthesis Laboratory, Institute for Atmospheric and Earth System Research/Forest Sciences, University of Helsinki, Helsinki, Finland

Abstract Novel satellite measurements of solar-induced chlorophyll fluorescence (SIF) can improve our understanding of global photosynthesis; however, little is known about how to interpret the controls on its spectral variability. To address this, we disentangle simultaneous drivers of fluorescence spectra by coupling active and passive fluorescence measurements with photosynthesis. We show empirical and mechanistic evidence for where, why, and to what extent leaf fluorescence spectra change. Three distinct components explain more than 95% of the variance in leaf fluorescence spectra under both steady-state and changing illumination conditions. A single spectral shape of fluorescence explains 84% of the variance across a wide range of species. The magnitude of this shape responds to absorbed light and photosynthetic up/down regulation; meanwhile, chlorophyll concentration and nonphotochemical quenching control 9% and 3% of the remaining spectral variance, respectively. The spectral shape of fluorescence is remarkably stable where most current satellite retrievals occur (“far-red,” >740nm), and dynamic downregulation of photosynthesis reduces fluorescence magnitude similarly across the 670- to 850-nm range. We conduct an exploratory analysis of hourly red and far-red canopy SIF in soybean, which shows a subtle change in red:far-red fluorescence coincident with photosynthetic downregulation but is overshadowed by longer-term changes in canopy chlorophyll and structure. Based on our leaf and canopy analysis, caution should be taken when attributing large changes in the spectral shape of remotely sensed SIF to plant stress, particularly if data acquisition is temporally sparse. Ultimately, changes in SIF magnitude at wavelengths greater than 740 nm alone may prove sufficient for tracking photosynthetic dynamics.

Plain Language Summary Satellite remote sensing provides a global picture of photosynthetic activity—allowing us to see *when*, *where*, and *how much* CO₂ plants are assimilating. To do this, satellites measure a small emission of energy from the plants called chlorophyll fluorescence. However, this measurement is typically made across a narrow wavelength range, while the emission spectrum (650–850 nm) is quite dynamic. We show *where*, *why*, and *to what extent* leaf fluorescence spectra change across a diverse range of species and conditions, ultimately informing canopy remote sensing measurements. Results suggest that wavelengths currently used by satellites are stable enough to track the downregulation of photosynthesis resulting from stress, while spectral shape changes respond more strongly to dynamics in canopy structure and chlorophyll concentration.

1. Introduction

There is a critical need to improve the mapping and monitoring of terrestrial photosynthesis to inform global carbon budgets (Schimel et al., 2015). Oxygenic photosynthesis converts solar radiation to chemical energy, sustaining nearly all higher life-forms on Earth. Photons captured by leaf chlorophyll have three primary fates: they can drive photosynthesis (photochemical quenching, PQ), be dissipated as heat (nonphotochemical quenching, NPQ), or be emitted as chlorophyll *a* fluorescence (ChlF). An analysis of the emission of

Harrington, Jerry Hatfield, Ying Sun, Albert Porcar-Castell

Methodology: Troy S. Magney, Christian Frankenberg, Gretchen North, Thomas S. Davis, Christian Dold, Debsunder Dutta, Joshua B. Fisher, Katja Grossmann, Alexis Harrington, Jerry Hatfield, Jochen Stutz, Albert Porcar-Castell

Project administration: Christian Frankenberg, Jerry Hatfield

Resources: Troy S. Magney, Christian Frankenberg, Gretchen North, Thomas S. Davis, Albert Porcar-Castell

Software: Katja Grossmann, Jochen Stutz

Supervision: Christian Frankenberg, Gretchen North, Joshua B. Fisher, Jochen Stutz, Albert Porcar-Castell

Validation: Troy S. Magney

Writing - original draft: Troy S. Magney, Christian Frankenberg, Gretchen North, Joshua B. Fisher, Ying Sun, Albert Porcar-Castell

Writing - review & editing: Troy S. Magney, Christian Frankenberg, Gretchen North, Thomas S. Davis, Christian Dold, Debsunder Dutta, Katja Grossmann, Alexis Harrington, Jerry Hatfield, Jochen Stutz, Ying Sun, Albert Porcar-Castell

photons in the 650- to 850-nm ChlF range provides information on light utilization at subcellular and leaf scales (Baker, 2008; Krause & Weis, 1991). Leaf-level ChlF is typically integrated over a broad spectral region using pulse-amplified modulation (PAM) instruments (Schreiber et al., 1986). Since PAM fluorometry measures the fluorescence response to a weak modulated light (ML) source, the magnitude of fluorescence can be decoupled from reflected radiation and effectively provide a fluorescence yield (ΦF_t). Further, PAM fluorometry uses short saturating light pulses to close photosystem II (PSII) and thereby enable the determination of PQ and NPQ of absorbed photons (Krause & Weis, 1991). For these reasons, PAM fluorometry has been a valuable tool in plant ecophysiology research—but is restricted to the leaf scale—spurring efforts to scale ChlF to larger scales from remote sensing platforms (Meroni et al., 2009; Albert Porcar-Castell et al., 2014).

Recent advances in the remote sensing of solar-induced ChlF (SIF)—indicative of the product of $\Phi F_{t,\lambda}$ and absorbed photosynthetically active radiation (APAR)—show promise for mapping plant photosynthetic dynamics globally (Frankenberg et al., 2011; Guanter et al., 2014; Joiner et al., 2011; Sun et al., 2018, 2017). However, the direct connection between PAM ChlF, remotely sensed SIF, and photosynthesis is lacking. Here, we define leaf-level ChlF as $F_{t,\lambda}$, and canopy-level ChlF as SIF_λ , both measuring the absolute radiant energy flux of ChlF from remote sensing platforms (e.g., $W \cdot m^{-2} \cdot nm^{-1} \cdot sr^{-1}$; equation (1)):

$$F_{t,\lambda}, SIF_\lambda = APAR * \beta_\lambda * [(f_{PSII} * \Phi_{PSII} * S_{\lambda,PSII}) + ((1-f_{PSII}) * \Phi_{PSI} * S_{\lambda,PSI})] \quad (1)$$

where APAR is absorbed photosynthetically active radiation ($\mu mol \cdot m^{-2} \cdot s^{-1}$), β_λ is the spectrally dependent leaf or canopy escape probability, f_{PSII} is the fraction of photons absorbed by PSII photosystems, Φ is fluorescence yield of PSII and PSI (quanta emitted/quanta absorbed), and S is the spectral shape of PSII and PSI ($J \cdot \mu mol^{-1} \cdot nm^{-1} \cdot sr^{-1}$). In contrast, steady-state fluorescence from PAM (F_t), typically recorded in millivolts, can be expressed as

$$F_t = APAR_{ML} * \beta_{f_{650-850}} * \left[(f_{PSII} * \Phi_{PSII} * S_{f_{650-850,PSII}}) + ((1-f_{PSII}) * \Phi_{PSI} * S_{f_{650-850,PSI}}) \right] * c \quad (2)$$

where $APAR_{ML}$ is the absorbed radiant energy from a fixed output ML and the wavelength dependency of β and S is simply measured as the integral of emitted fluorescence somewhere in the 650- to 850-nm range (depending on the manufacturer; Magney, Frankenberg, et al., 2017), while c is a factor that accounts for the preset sensitivity of the photodiode ($mV/[W \cdot m^{-2} \cdot nm^{-1} \cdot sr^{-1}]$). The spectral shape (S) of ChlF has two peaks centered in the red (~685nm) and far-red (~740 nm) spectrum, with nonequal contributions from PSI and PSII. PSII exhibits variable fluorescence across the ChlF spectrum as its yield is affected by PQ and NPQ (Franck et al., 2005; Lambrev et al., 2010); PSI generally has a lower yield and is assumed to be constant (not impacted by changes in NPQ and PQ; Franck et al., 2002; Hasegawa et al., 2010). Since PSI contributes very little to red ChlF (~685 nm), red wavelengths are thought to be more responsive to environmental stress (downregulation of photosynthesis) compared to far-red fluorescence—where PSI contributes a potentially significant fraction to the total SIF signal.

The magnitude and spectral shape of leaf ChlF are known to change with irradiance conditions (Pinto et al., 2016), chlorophyll concentration (Buschmann, 2007; Gitelson et al., 1998; Hak et al., 1990; Lichtenthaler et al., 1990), physiological condition (PSI/PSII contributions, NPQ; Franck et al., 2005, 2002; Lambrev et al., 2010; Palombi et al., 2011; Rizzo et al., 2014), temperature (Agati, 1998; Croce et al., 1996), photosystem stoichiometry and structure (Farooq et al., 2018; Johnson et al., 2005), and leaf optical properties (Gitelson et al., 1998; Vilfan et al., 2016). At steady state, a large body of research suggests that deviations in the red (~685 nm) to far-red (~750 nm) ChlF ratio are controlled by Chl concentration, which regulates the degree of reabsorption in the red part of the spectrum along the escape path of the photon (Buschmann, 2007; Gitelson et al., 1998; Lichtenthaler et al., 1990). By accounting for changes in the spectral shape due to Chl reabsorption, researchers have suggested that the red:far-red ChlF ratio can potentially provide information on the responses of vegetation to water, temperature, or nitrogen stresses (Ač et al., 2015; Agati, 1998; Buschmann, 2007; Genty et al., 1990; Lichtenthaler et al., 1998). Building on this, some canopy-scale research indicates that large diurnal changes in the remotely sensed red:far-red SIF ratio can be attributed to the downregulation of photosynthesis (Ač et al., 2015; Middleton et al., 2017; Wieneke et al., 2016, 2018); but note that this may be overshadowed by canopy structure and measurement geometry effects

(Goulas et al., 2017; Liu et al., 2018). However, we are not aware of any attempts to disentangle contributing factors (i.e., Chl and changes in PSI/PSII fluorescence contributions), which simultaneously impact the spectral shape of ChlF ratio on single leaves.

Additionally, challenges remain regarding how the nonlinear relationships between photosynthesis, NPQ, and ChlF at the leaf scale affect SIF at the canopy scale (Porcar-Castell et al., 2014; van der Tol et al., 2014). Current SIF retrievals in discrete and narrow wavelength bands appear to track the dynamics of photosynthesis at a wide range of spatial scales (Rascher et al., 2015; Sun et al., 2017; Wieneke et al., 2016; Yang et al., 2015; Magney et al., 2019) but are mostly restricted to spectral windows around 750 nm, with attempts to derive independent estimates of SIF at 680 nm (Joiner et al., 2016). Future missions propose to retrieve the full SIF spectrum (Drusch et al., 2016; Zhao et al., 2018), which could be useful for better constraining photosynthetic efficiencies if the controls on the ChlF spectral shape at both leaf and canopy scales are well understood. This is particularly important as satellite measurements made at one time during the day will need to decouple covarying contributions to the ChlF spectral shape related to canopy biochemistry, physiology, and structure.

Here, we test the potential for disentangling contributions to the shape of the ChlF spectrum at the leaf scale and investigate how these results manifest at the canopy scale. We use a recently developed instrument to measure PAM and spectrally resolved ChlF simultaneously in a controlled leaf chamber (Magney, Frankenberg, et al., 2017), which reveals the response of the ChlF spectral shape to changes in physiological and environmental conditions. A singular-value decomposition (SVD) of ChlF spectra at the leaf scale ($F_{t,\lambda}$) informs our interpretation of red:far-red ChlF at the canopy scale (SIF) and allows us to study *where*, *why*, and *to what extent* the ChlF spectrum changes under three different scenarios:

1. *Across and within species at steady-state: Leaf-scale.* We disentangle the effects of chlorophyll and photochemistry on ChlF spectra by sampling a range of species from the tropics, boreal forest, cropping systems, and a temperate botanical garden. This experiment informs our understanding of how steady-state $F_{t,\lambda}$ spectra might vary *spatially* (across species) and *seasonally* (within species).
2. *Under varying illumination conditions: Leaf-scale.* We run leaves through a light response curve to assess changes associated with a wide range of light-induced PQ, NPQ, and photosynthesis for different leaves. This experiment allows us to investigate how spectral shapes vary in *time*—over the course of a day—as would be observed from a stationary satellite platform.
3. *Diurnal and seasonal changes in remotely sensed SIF: Canopy scale.* To bridge the gap between leaf and canopy spectral dynamics, we highlight daily and seasonal changes in the red:far-red SIF ratio as observed from a tower system at a soybean field and discuss the covarying controls (chlorophyll, canopy structure, photosynthetic downregulation, and canopy structure) on this ratio.

2. Materials and Methods

2.1. Leaf Samples and Ancillary Data

Leaf samples were collected from four locations: (1) the Huntington Library and Botanical Gardens in Pasadena, CA; (2) La Selva Biological Station in Puerto Viejo de Sarapiquí, Costa Rica; (3) Hyttiälä Forestry Field Station in Finland; and (4) grown in a greenhouse at California Polytechnic State University, San Luis Obispo (Cal Poly). Details on species, sampling, and growth conditions can be found in Table S1 in the supporting information. Leaves from both sunlit and shaded canopy positions were collected to ensure a wide range of growth conditions. For each sample, terminal branches (or shoots) with 3–10 leaves were removed from each plant, immediately placed and recut under water prior to a >20-min dark adaption. In this study only leaves exhibiting mild chlorosis were included so as to not conflate analysis with senesced leaves (Lichtenthaler et al., 1998). Prior to insertion into the leaf cuvette, Chl concentration was collected using an Apogee Chlorophyll Concentration Meter (Apogee Instruments, Logan, UT). The average Chlorophyll Concentration Meter value after three samples was then converted to absolute units ($\mu\text{mol}/\text{m}^2$) following Parry et al. (2014). Note that Chl concentration measurements were only conducted on the Huntington, La Selva, and Cal Poly data sets. Further, we estimate the fraction of absorbed photosynthetically active radiation ($f\text{APAR}$) value by computing leaf reflectance in the red (at 630 nm) and leaf transmittance using an exponential function to convert Apogee chlorophyll concentration to transmittance according to equation (3):

$$f\text{APAR}_{\text{red}} = 1 - \left[\left(\text{Rad}_{630,\text{leaf}} / \text{Rad}_{630,\text{spectralon}} \right) + \exp(-\text{Chl} / \text{Chl}_{\text{max}}) \right] \quad (3)$$

where Rad is reflected radiance ($\text{W} \cdot \text{m}^{-2} \cdot \text{s}^{-1}$) from the leaf surface and a white reference panel (Spectralon, Labsphere, North Sutton, NH, USA), and Chl is the Chl concentration value computed via transmittance from the Apogee instrument. In the computation of equation (3), we make the assumption that the exponential function accurately describes the fraction of transmitted radiation and that these values are comparable across samples, similar to equation (5).

2.2. Leaf-Level Instrumentation

The analysis was done using the instrument and spectral nomenclature described in (Magney, Frankenberg, et al., 2017) (Table S2), which includes a coupled fiber optic that simultaneously records PAM and spectral information under the same field of view in an environmentally controlled cuvette. The bundled foreoptic was at an angle of 60° and 2 mm to the leaf, with an identical field-of-view (FOV) between the PAM and spectral data. The instrument also includes a short-pass filter below the incident light source, attenuating light above 675 nm to isolate the complete ChlF spectrum >675 nm from reflected light. A bank of 90% red and 10% blue LEDs was used as the incident light source to ensure that light quantity and quality was equal across all samples. While the dominance of red light is not ideal for extrapolating these findings to SIF remote sensing, we show that the primary variance in the spectra from red, blue, and white light is within 5% (Figure S1 and S2). For all samples, ambient CO_2 concentration (varying from 380–420 ppm), a relative humidity of 50%, flow rate of $600 \mu\text{mol/s}$ and cuvette temperature of 25°C were used. All measurements were made on the upper (adaxial) side of the leaf or needle, the latter of which were configured in “needle mats” (Rajewicz et al., 2019).

The manufacturer-provided PAM-Fluorimeter 3050-F was used to determine ChlF parameters (Heinz Walz GmbH) using a blue LED saturating pulse of $6,000 \mu\text{mol} \cdot \text{m}^{-2} \cdot \text{s}^{-1}$ for 0.8 s. NPQ was calculated as $(F_m - F_{m'}) / F_m$, where F_m is maximal fluorescence in the dark, and $F_{m'}$ is maximal fluorescence in the light. PQ was calculated as $(F_m / F_t) - (F_m / F_{m'})$, where F_t is transient fluorescence measured by the 500-Hz blue modulating light. Spectral measurements were collected using a QE Pro high sensitivity spectrometer (Ocean Optics, Dunedin, FL, USA) with a range of 474–858 nm and spectral sampling of 0.35 nm. Spectra were recorded every 0.2 s from co-adding 20 spectra using a 10-ms integration time. To compare steady-state spectra ($F_{t,\lambda}$) during the light response curve to ancillary variables, a 5-s average of $F_{t,\lambda}$ data immediately prior to each saturation pulse was used, at which point transient fluorescence had reached a steady state. All measurements were done in a darkened lab to ensure that light from other sources would not enter the leaf chamber. Calculation of all PAM and spectral variables can be found in Table S2. For the soybean stress experiment, gas-exchange data were collected to measure net photosynthetic assimilation (A_{net}). The GFS-3000 uses two calibrated infrared gas analyzers to calculate a difference in CO_2 and H_2O concentrations in a reference and a sample cell during measurements, and photosynthesis was recorded after samples has reached a steady-state at each light level.

2.3. Experiment 1: Variability in ChlF Spectrum at Steady State Across and Within Species

To determine the primary modes of variability in the ChlF spectrum at steady state, we compared ChlF spectra ($F_{t,\lambda}$) across a range of 27 species at a PAR of $600 \mu\text{mol} \cdot \text{m}^{-2} \cdot \text{s}^{-1}$. Each sample was dark adapted for >20 min, after which minimal fluorescence (F_0) and a saturation pulse were recorded to estimate maximal fluorescence (F_m) and variable fluorescence ($F_v / F_m = (F_m - F_0) / F_m$). Following the recording of F_m , the actinic LED light bank was turned on and a saturation pulse was recorded every 30 s (Atherton et al., 2017) to capture NPQ and PQ dynamics. After 4 min of exposure at $600 \mu\text{mol} \cdot \text{m}^{-2} \cdot \text{s}^{-1}$ PAR, a 1-min average of $F_{t,\lambda}$ data was used to produce the steady-state spectral shape. For the across-species experiment, an NPQ and PQ value after 5 min was used. Individuals were not grouped by species so the variance of all individual leaf samples could be accounted for (Table S1). To compare the spectral variability across all individuals, a SVD (see section 2.7) was performed on the 675- to 850-nm range for $F_{t,\lambda}$, because the red LED spectrum influences the lower range of ChlF wavelengths in $F_{t,\lambda}$ spectra up to a short-pass filter at 675 nm between leaf samples and the LED unit (Magney, Frankenberg, et al., 2017). Note that the fiber calibration used during the Hyytiälä campaign differed slightly from the rest of the measurements, so these data were not included in the SVD analysis. A narrative of the SVD analysis across four example species can be found in Figure S3.

We also conducted a within species experiment to evaluate the wide range of conditions a single species may experience over the course of the season. This analysis was conducted for three common agricultural plants: *Zea mays* (corn), *Glycine max* (soybean), and *Brassica oleracea* (broccoli). Each species was grown in the greenhouse and received different amounts of water (Text S1). Measurements of each sample at $600 \mu\text{mol}\cdot\text{m}^{-2}\cdot\text{s}^{-1}$ PAR (to match the across-species experiment) were made across all water conditions for each species and individual. Complete light response curves are presented for the soy plants exposed to stress to compare the impact of changing fluorescence shape against net photosynthesis (Text S1). To validate our empirical data, we use known absorption features in a modeling framework (Text S2). A more detailed discussion on the methods associated with the modeling framework and experimental design can be found in the supporting information (Davis et al., 2015; van der Tol, Verhoef, & Rosema, 2009; van der Tol, Verhoef, Timmermans, et al., 2009).

2.4. Experiment 2: Variability in Steady-State ChlF Under Different Illumination Conditions

An SVD analysis during the course of a light-response curve (LRC) gives us information on the expected variance of the ChlF spectrum driven by changes in illumination. A similar analysis to experiment 1 was conducted for individuals from the Hyytiälä campaign (see section 2.1) during an LRC. Sampling conditions within the leaf cuvette were identical to previous experiments, except for the changes in PAR. The LRC protocol consisted of exposing a sample to 1,200, 800, 400, 200, 100, 50, and $25 \mu\text{mol}\cdot\text{m}^{-2}\cdot\text{s}^{-1}$ of actinic light PAR until a steady state was reached at each light level (where negligible changes in NPQ or PQ were observed). $F_{t,\lambda}$ data were averaged for 5 s prior to each saturation pulse. A saturation pulse was recorded at the end of each light level, when the sample was presumed to be at steady state based on negligible observed changes in F_t from the PAM data. SVD sample weights, singular values, and principal components (PCs) were compared across 18 individuals from five different species from Hyytiälä. The leaves and needles came from upper and lower canopy locations and were all in their second year of growth, detailed information in Table S1. To validate changes in the shapes observed during the LRC, we conducted a rapid photosynthetic light induction (Kautsky curve) experiment (Text S3 and Figure S4). A more detailed discussion on the methods associated with the rapid photosynthetic light induction experiment and its design can be found in the supporting information (Kautsky & Hirsch, 1931; Kitajima & Butler, 1975; Lazar, 1999; Stirbet & Govindjee, 2011).

To build on our leaf-level analysis, we show canopy level SIF data across a growing season in a soybean field. Canopy spectroscopic retrievals of SIF are done using a two-step least squares retrieval procedure within the solar Fraunhofer lines and have a high signal-to-noise ratio, permitting retrievals in the red (680–686) and far-red (745–758 nm) spectral region under all atmospheric conditions (Grossmann et al., 2018). While both canopy and leaf level ChlF data are passively collected, we recognize that emitted ChlF as measured in the laboratory is not truly SIF and is thus referred to as $F_{t,\lambda}$ throughout, while SIF only refers to canopy level measurements.

2.5. Experiment 3: Dynamics in Canopy Red:Far-Red SIF Using Tower Spectroscopy Data

Data from a scanning-spectrometer (PhotoSpec) atop a 7-m tower were used for the canopy-scale analysis. The PhotoSpec was deployed just after planting at a soybean field near Ames, IA, USA, in late May 2017 and remained until just prior to harvest in September 2017. The field is on a soybean-corn rotation near the Brooks Field AmeriFlux tower (<https://ameriflux.lbl.gov/sites/siteinfo/US-Br3>). The farming system, tillage, and nutrient management practices are typical for those in the Upper Midwest Corn-Belt (more details can be found in Dold et al., 2019).

The detection of SIF is based on measuring change in the optical density of a well-known narrow spectral feature in the presence of a ChlF signal, a solar Fraunhofer line (Carter et al., 1990; Fraunhofer, 1817; Plascyk & Gabriel, 1975). As is described in Grossmann et al. (2018), the retrieval of SIF requires a spectrometer with excellent thermal stability, high spectral resolution, and high signal-to-noise ratios to discern SIF from reflected sunlight. The instrumental setup and retrieval algorithm are based on Differential Optical Absorption Spectroscopy (Platt & Stutz, 2008), an established method to measure atmospheric trace gases. The PhotoSpec instrument consists of a two-dimensional (2-D) scanning telescope unit, which can be pointed to any location on a canopy at user selectable azimuth and elevation angles. Light reaching the telescope is distributed into three thermally stabilized commercial spectrometers via optical fiber bundles. These

spectrometers cover wavelength ranges at high spectral resolution to retrieve SIF in the red and far-red wavelength range, as well as at moderate resolution to retrieve vegetation indices such as the normalized difference vegetation index (NDVI), the photochemical reflectance index (PRI), and a remotely sensed chlorophyll index (Chlorophyll_{RS}; Table S3 and Text S4). More detailed information on vegetation indices can be found in the supplementary information, Text S4 (Datt, 1999). The telescope unit also includes a commercial PAR sensor (LI-COR LI-190R, Lincoln, Nebraska, USA). A typical measurement sequence in the field starts with the measurement of a solar reference spectrum using an upward-looking opal glass diffuser, followed by a scan from nadir to the horizon in 0.7° steps at two different azimuth directions, with a time resolution of approximately 20 s per measurement. The PhotoSpec also has a 0.7° FOV, making for a ~5- to 20-cm diameter footprint on the top of the canopy. The return interval for a complete scan is around 20 min, but we average data from all scans on an hourly time resolution to match the temporal resolution of flux tower data, and to mimic a satellite retrieval with a larger FOV, which would capture all sunlit and shaded canopy components. Further details on the PhotoSpec instrument and retrieval process can be found in Text S4.

2.6. Eddy Covariance Data

Net Ecosystem Exchange (NEE) data were collected at an eddy covariance flux tower located in the same field as the PhotoSpec instrument and provided by the U.S. Department of Agriculture National Laboratory for Agriculture and the Environment (Ames, IA). GPP flux partitioning was performed using the REdDyProc tool (Wutzler et al., 2018). The partitioning is achieved by postprocessing half-hourly data sets of NEE together with ancillary meteorological data of friction velocity, global shortwave radiation, air or soil temperature, and vapor pressure deficit. The processing steps consist of (i) filtering of periods with low turbulent mixing, (ii) gap filling of missing data sets, and (iii) partitioning NEE into GPP and respiration fluxes. For the present study nighttime flux partitioning method (Reichstein et al., 2005) using temporally varying respiration-temperature relationship from nighttime data is used.

2.7. Statistical Analysis

Using our extensive data set of simultaneously recorded active and passive fluorescence, we assemble measurements into a two-dimensional matrix A with n rows and m columns, where n is the number of species/samples and m is the number of spectral points. Using SVD, we can factorize A into three matrices $A = USV^T$, where the columns of U and V are the left- and right-singular vectors of A , and S is a rectangular diagonal matrix with positive entries representing the singular values (s_i) in descending order. The matrix A containing the ChlF spectra ($F_{t,\lambda}$) can then be perfectly reconstructed by a linear superposition of all left- and right-singular vectors scaled by the corresponding singular values:

$$A = F_{t,\lambda} = \sum_{i=1}^n \mathbf{u}_i * s_i * \mathbf{v}_i^T \quad (4)$$

where u_i is the i th left singular vector (length n) containing individual sample weights, v_i is the right singular vector (length m) containing the i th PCs (PC_{*i*}, equivalent to spectral shapes), and s_i is the singular value of the i th component. Typically, only a few components are needed to reconstruct A with sufficient accuracy, explaining most of the variance in $F_{t,\lambda}$. However, these main components are mathematically derived and not necessarily related to physical processes. To interpret the PCs in terms of controlling factors, we also performed an SVD on a synthetic dataset, in which we vary contributions from PSI and PSII as well as chlorophyll absorption in a simple model for $F_{t,\lambda}$:

$$F_{t,\lambda} = (x_1 * \text{PSI}_\lambda + x_2 * \text{PSII}_\lambda) * T_\lambda \quad (5)$$

where T is the wavelength-dependent leaf transmission, estimated as $\exp(-x_3 * \text{Chl}_{a,b} \text{ absorbance})$, and $x_{1,2,3}$ represent contributions from PSI, PSII, and Chl_{*a,b*} content, respectively.

The SVD approach is applied in many branches of science to reduce the dimensionality of data sets. In some cases, it is even possible to attach a physical meaning to the reduced dimensions (PCs), which result from a decomposition of data in orthogonal directions. In this analysis however, we try to ascribe empirical relationships between PC sample weights and ancillary variables. From (4), the columns of V and U always form an orthogonal set, making no assumptions on the $F_{t,\lambda}$ matrix. The SVD finds the best fitting line through the data by minimizing the sum of squared distances perpendicular to the least squares line of best fit in each

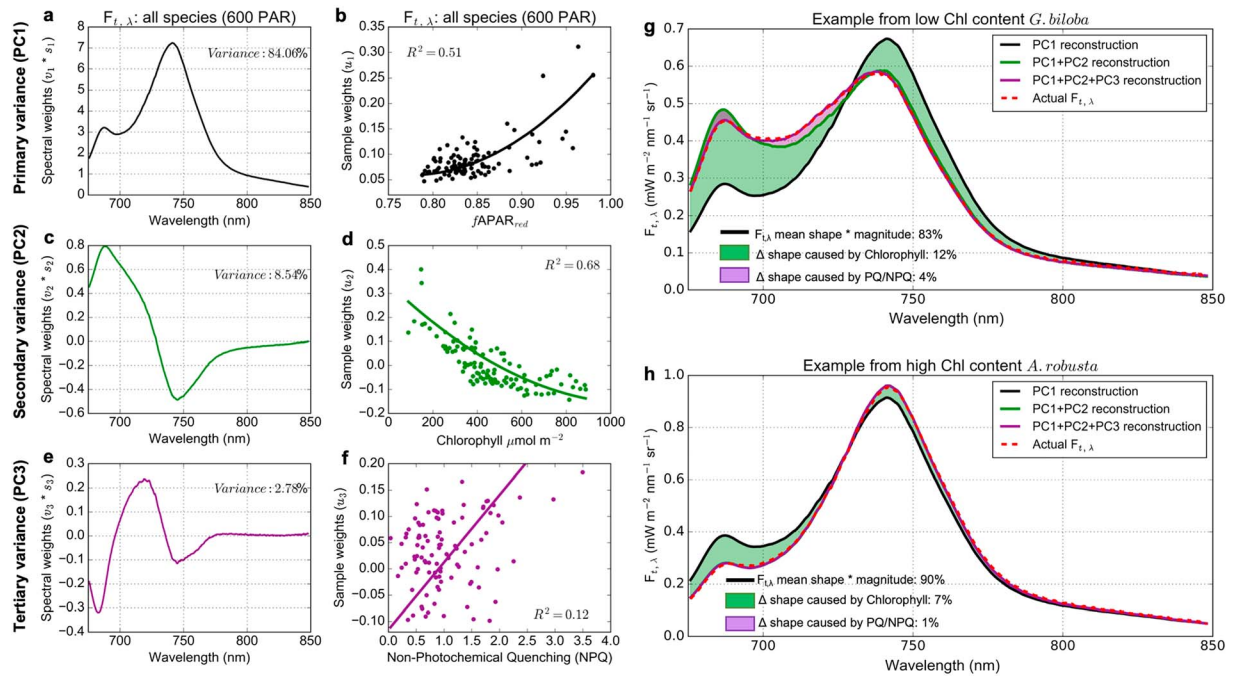


Figure 1. Spectral variance across species. (a, c, and e) Spectral variance associated with PCs 1, 2, and 3, respectively. Spectral weights are provided in absolute radiance units ($v_n * s_n$; $\text{mW} \cdot \text{m}^{-2} \cdot \text{nm}^{-1} \cdot \text{s}^{-1}$). The total explained variance of each PC across all species is in the subplot text. (b, d, and f) PC_n sample weights (u_n) represent the relative influence each sample has on the direction and magnitude of the PC_n spectral shape, and are shown against empirical variables: (b) Fraction of absorbed photosynthetically active radiation ($fAPAR_{red}$); (d) chlorophyll concentration ($\mu\text{mol}/\text{m}^2$); (f) Nonphotochemical quenching (NPQ). In (b) and (d), a second-order polynomial is fit to the data by minimizing the variance of the coefficients using a least squares approach, and a linear least squares fit in (f). (g and h) Linear reconstruction of ChlF spectra from the top three PCs using two examples of species with low Chlorophyll content, *G. biloba* (g), and high, *A. robusta* (h). The explained variance of each PC can be found in the subplot text, with shaded regions indicating the change (Δ) associated with each additive PC spectral weight * sample weight. PQ = photochemical quenching; PC = principal component.

dimension (k). For each PC, we can then compute the explained variance with respect to the underlying data set according to equation (6):

$$\text{Explained variance}_k = \frac{S_k}{\sum_{k=1}^n S_k} \quad (6)$$

The rows of the left singular vectors associated with each PC (sample weights [u]) provide us with the relative influence each data point (n) has on the PC. We can compare these values with potential explanatory variables, such as Chl concentration, PQ, and NPQ, in order to empirically attach a biophysical meaning to the PCs.

3. Results

3.1. ChlF Variability Across Species: Leaf-Scale

Three leading spectral components explain 95.4% of the variance in the ChlF spectra across all species (Figure 1). As expected, the first PC (PC1) represents the mean spectral shape across all species (Figure 1a), while the sample weights represent the magnitude of ChlF (Figure 1b). $F_{t,\lambda}$ magnitude increases with $fAPAR_{red}$, but the nonlinearity is likely due to variations in $\Phi F_{t,\lambda}$, which is modulated by both PQ and NPQ (Figure 1b). PC2 (Figure 1c) explains 8.5% of the variance and is dominated by changes in the red region of the spectrum, where Chl molecules reabsorb fluoresced photons. Measured Chl concentration across individual leaves corresponds to this spectral shape ($R^2 = 0.68$; Figure 1d). To third order, PC3 explains 2.8% of the variance (Figure 1e) and shows a positive trend accompanying NPQ (Figure 1f). Across all species, the linear superposition of only three PCs results in the near complete reconstruction

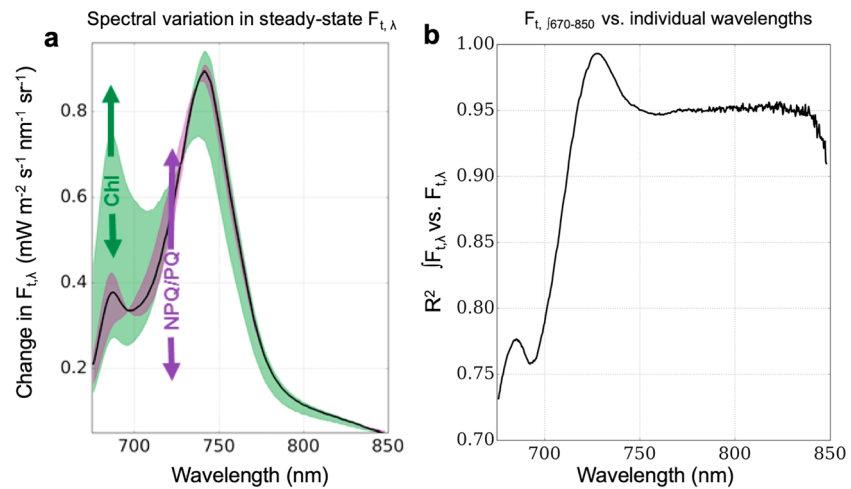


Figure 2. Summary of expected changes in the ChlF emission spectrum from across species at steady state (from Experiment 1). (a) The expected spectral changes in radiance units associated with PC2 and PC3, the first, which we attribute to changes in chlorophyll concentration (green), and the latter which we attribute to changes in NPQ (purple). The solid line refers to the mean spectral shape across all samples. (b) Coefficient of determination for all wavelengths against the integral of the ChlF emission spectrum for all leaves from Experiment 1. Taken together, these results suggest that the far-red part of the spectrum is quite stable and that the spectral region between 675 and 730 nm is where most of the change in the spectral shape of ChlF occurs. PC = principal component.

of each individual leaf's ChlF spectrum (>98% explained variance for each leaf, examples shown in Figures 1g and 1h). We find that the far-red region of the spectrum is remarkably stable and its magnitude (>740 nm) is tightly correlated to the integral of the entire ChlF spectrum across all samples (Figure 2). Lastly, no species- or plant functional type-specific clustering from a PC2 versus PC3 biplot was observed, suggesting that changes in the shape of the ChlF spectra are likely not dominated by differences in leaf morphology within individual species (Figure S5); however, leaf structure and optical properties will have an impact on the fraction of ChlF escaping the leaf (PC1), which we cannot account for in this study (Johnson et al., 2005; Vilfan et al., 2016).

3.2. ChlF Variability Within Species: Leaf-Scale

To further investigate the spectral changes within individual species, we compared leaves of *Zea mays* (corn), *Glycine max* (soybean), and *Brassica oleracea* (broccoli) grown in a greenhouse under high, medium, and low water conditions (Figure 3). This experiment shows how the spectral shape might change during the course of a season, where a range of pigments and stress levels may be expressed.

The primary, secondary, and tertiary variance in spectral shapes (Figures 3a, 3c, and 3e) are nearly identical to those observed in the across-species experiment (Figure 1). The explained variance of PC1 ranges from 85–89%, 5–8% for PC2, and 1–2% for PC3 across all three species. We find strong relationships between PC1 sample weights and $f\text{APAR}_{\text{red}}$ (Figure 3b), PC2 and Chl concentration (Figure 3d), and PC3 and NPQ (Figure 3f). To validate the empirical correlations between sample weights and ancillary data, we created a simple synthetic model by modifying Chl concentration and PSI/PSII contributions from known Chl absorption spectra and derived PSI/PSII shapes (van der Tol, Verhoef, & Rosema, 2009; van der Tol, Verhoef, Timmermans, et al., 2009). The model reproduces a similar PC2, driven by changes in reabsorption by Chl, and PC3 by relative PSI/PSII contributions (Figure S6), supporting our mechanistic hypothesis.

3.3. ChlF Under Varying Illumination: Leaf-Scale

For individual leaves exposed to changing light levels, the mean shape of the spectrum explains over 98% of the variance in the spectrum (Figure 4a) and its magnitude is, as expected, tightly coupled to changes in $\Phi F_{t,\lambda} * \text{PAR}_{\text{red}}$ ($R^2 = 0.94$; Figure 4b). Across all LRCs, changes in the spectral shape only accounts for 1–2% of the variance, with a consistent pattern across all individuals (Figure 4d). The sample weights associated with

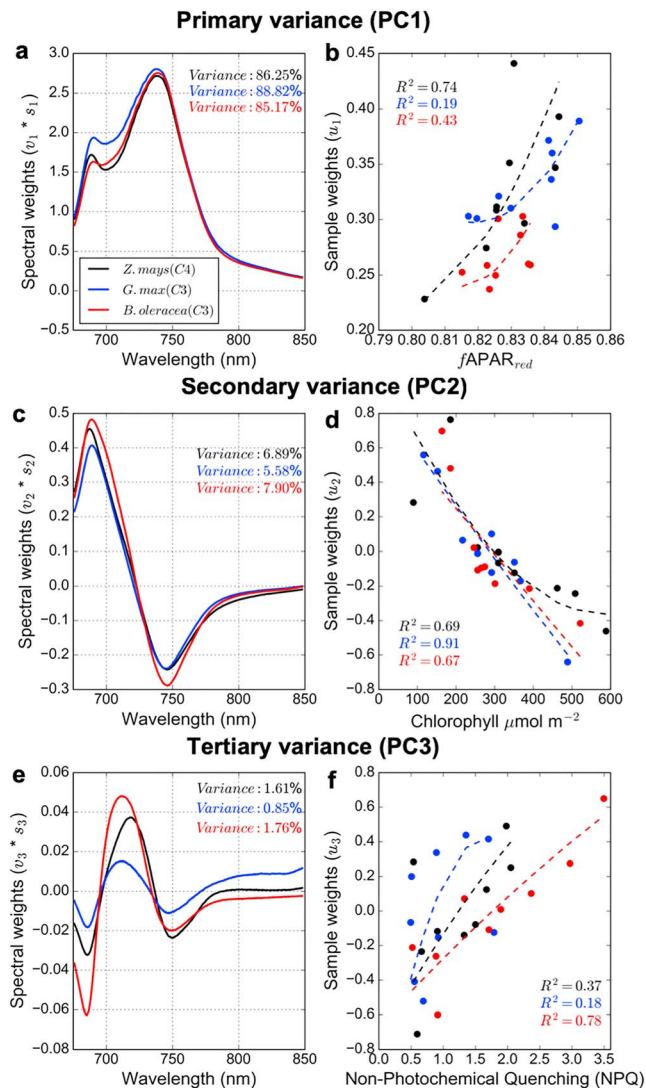


Figure 3. Spectral variance within species. (a–f) *Zea mays* (black), *Glycine max* (blue), and *Brassica oleracea* (red). (a, c, and e) Spectral variance associated with PCs 1, 2, and 3, respectively for each species, and explained variance in the subplot text. Spectral weights are provided in absolute radiance units ($v_n \cdot s_n$, $\text{mW} \cdot \text{m}^{-2} \cdot \text{nm}^{-1} \cdot \text{s}^{-1}$). (b, d, and f) PC_n sample weights (u_n) represent the relative influence each sample has on the direction and magnitude of the PC_n spectral shape and are plotted against empirical variables: (b) fraction of absorbed photosynthetically active radiation ($fAPAR_{red}$); (d) chlorophyll concentration ($\mu\text{mol}/\text{m}^2$); (f) non-photochemical quenching (NPQ). In the right column, a second-order polynomial is fit to the data by minimizing the variance of the coefficients using a least squares approach. PC = principal component.

PC2 correspond to changes over time (and under varying light conditions) in NPQ ($R^2 = 0.86$; Figure 4e) to a greater degree than PQ (Figure 4f).

To validate that the spectral shape associated with PC2 is driven by changes in NPQ and PQ during the light response curve, we conducted an SVD analysis during rapid photosynthetic induction (i.e., the Kautsky effect, Figures S7 and S8). Fluctuations in ChlF spectra during this experiment represent the rapid quenching dynamics associated with changes in NPQ and PQ. During a 180-s exposure to high light after darkness, we find that the mean spectral shape (PC1) explains >97% percent of the variance across all individuals ($n = 48$) from 12 species (Figure S7). In this case, PC1 is not driven by APAR, but only by PQ and NPQ, representing the spectrally independent effect of NPQ and PQ, which is also present in the findings in Figure 4, but are masked by APAR. The shape of PC2 (Figures S7 and S8) is nearly identical to PC2 from the light-response curve experiment (Figure 4d) and explains about 2% of the variance.

3.4. Seasonal Trends in Canopy SIF

At the seasonal time scale, changes in daily red and far-red SIF magnitude show a similar pattern to both APAR and Gross Primary Production (GPP, Figure 5a), with stronger correspondence to changes in APAR (Figures 5b and 5c). The seasonal trends in red:far-red SIF are highest early and late in the season, and consistently low during peak greenness—negatively related to NDVI for most of the season, and positive during rapid vegetative growth (first 10 days; Figures 5d and 5e). This suggests that high red:far-red SIF ratios early in the season are likely the result of low green leaf area; meanwhile, Chl concentration (spectroscopically retrieved using the equation described in Datt, 1999) is high at this time—which we would expect to enhance the reabsorption of red photons at the leaf scale (Goulas et al., 2017). As the crop begins to senesce later in the season, the red:far-red SIF ratio also increases due to a depletion of Chl pigments (Figures 5e and 5f). Results suggest that both Chl concentration and canopy structure (NDVI, and accumulation of biomass) play a role in the seasonal red:far-red SIF trends, ultimately changing the quantity of red and far-red photons escaping the canopy (Figure S9). Reflected radiance in the same red to far-red regions as the SIF retrievals clearly indicate that red photons are more likely to escape the canopy early and late in the season (Figure S9a). Canopy radiative transfer models such as the Soil Canopy Observation, Photochemistry and Energy model help to understand the impacts of radiative transfer on our interpretation of the red:far-red ratio, with SIF contributions coming from both sunlit and shaded leaves, while scattered photons more readily escape the canopy in the far-red (Figure S10). Future work should seek to disentangle SIF contributions under changing radiative environments, which will ultimately aid in decoupling the “physical” from the “physiological” SIF signal.

3.5. Diurnal Trends in Canopy SIF

Considering the subtle change in red:far-red ChlF due to changes in NPQ at the leaf-scale, we investigated diurnal trends in this ratio at the canopy scale. Currently, the best remote sensing proxy of diurnal dynamics in NPQ is the PRI (indicative of a daily change in xanthophyll pigment interconversion (Gamon et al., 1992; Garbulsky et al., 2011; Magney et al., 2016). Both PRI and canopy light-use efficiency (LUE: $GPP/APAR$) are used to interpret diurnal dynamics in photosynthetic downregulation and red:far-red SIF. To first order, hourly averages in red and far-red SIF track APAR and GPP closely (Figures 6a–6c), and increases in both SIF and APAR generally correspond to a decrease in the red:far-red ratio (Figures 6b and 6c). On the hourly time scale, we see a similar midday

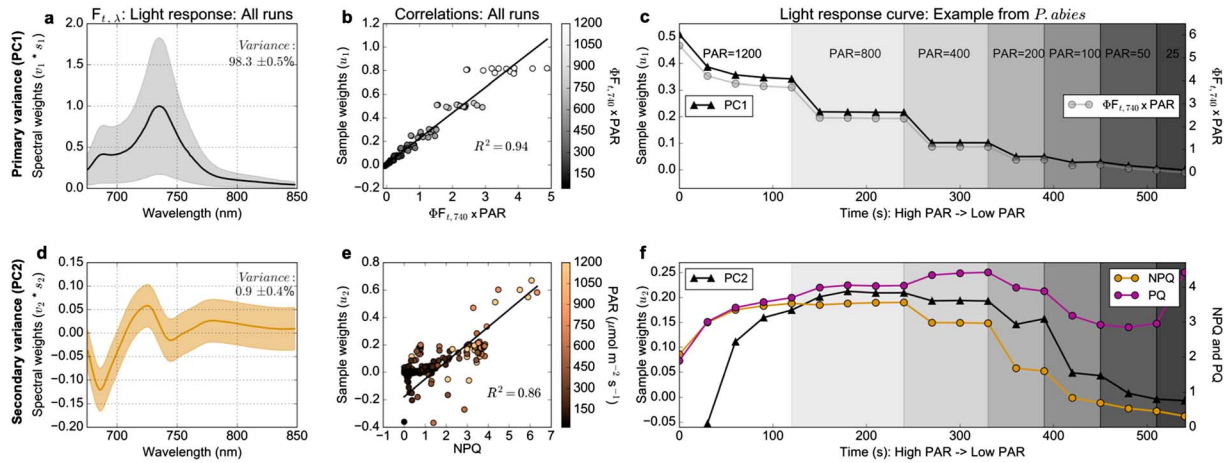


Figure 4. Spectral variance within individuals during light response curve. (a, d) Spectral variance associated with PCs 1 and 2, respectively. Spectral weights are provided in absolute radiance units ($v_n \cdot s_n, \text{mW}\cdot\text{m}^{-2}\cdot\text{nm}^{-1}\cdot\text{s}^{-1}$). The total explained variance of each PC across all species is in the subplot text. Solid curves represent the mean spectral shape across all individual sample runs, and shaded regions represent ± 1 standard error across all samples. (b, e) Sample weights from PC1 and PC2, representing the direction and relative magnitude of each sample on the spectral shape, against $\Phi F_{t,\lambda} \cdot \text{PAR}$ and nonphotochemical quenching (NPQ), respectively. (c, f) Example from one *P. abies* sample during the course of the light response curve. Shaded regions indicate incident PAR at the time of measurement. (c) Changes in PAR and fluorescence yield ($\text{PAR} \cdot \Phi F_{t,\lambda}$) with changes in PC1 sample weights. (f) Dynamics associated with changes in PC2, NPQ, and photochemical quenching (PQ) during the light response curve. PC = principal component.

decrease in LUE, red:far-red SIF, and the PRI (Figures 6d and S11). The decrease in red:far-red SIF is subtle and with considerable noise, while the day-to-day variation loosely corresponds to changes in both light (PAR) and photosynthetic downregulation (Figures 6d and S11). At peak greenness (25 July 25 and 5 September), when little day-to-day variation in red:far-red SIF occurs, far-red SIF tracks diurnal changes in LUE, where low red:far-red ratios correspond to low LUE (Figure 6e, $p < 0.05$). The red:far-red ratio does appear to track LUE during this time period (Figure 6d, $p < 0.05$), but most of this relationship is

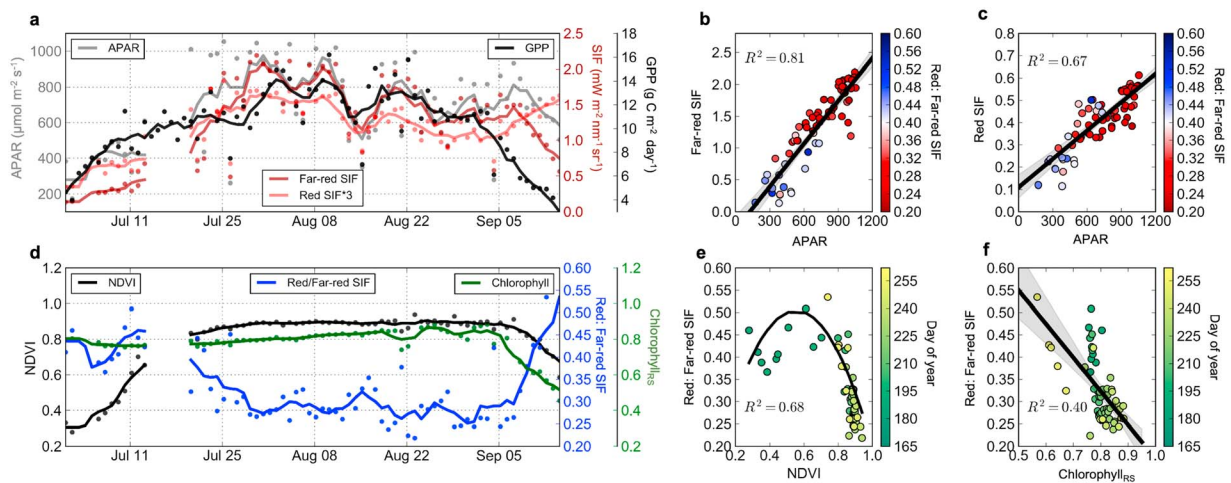


Figure 5. Seasonal dynamics of red SIF, far-red SIF, gross primary production (GPP), absorbed photosynthetically active radiation (APAR), red:far-red SIF, NDVI, and remotely sensed chlorophyll concentration ($\text{Chlorophyll}_{\text{RS}}$) as observed from a canopy spectrometer in soybean. (a) Total daily GPP (black), daily mean APAR (gray), daily mean far-red (dark red) and red SIF*3 (light red) over the course of the growing season. Dots represent individual days and lines a 5-day running mean. (b) Daily mean APAR against daily mean far-red SIF, colored dots represent the mean red:far-red ratio observed each day. (c) Mean daily APAR against red SIF; colored dots represent the daily mean red:far-red ratio. (d) Daily means (circles) and 5-day running means (lines) of $\text{Chlorophyll}_{\text{RS}}$ (green), NDVI (black) and red:far-red SIF (blue). (e) Correlation between NDVI and red:far-red SIF fit by a second-order polynomial colored by day of year. (f) Correlation between $\text{Chlorophyll}_{\text{RS}}$ and red:far-red SIF colored by day of year. NDVI = normalized difference vegetation index; SIF = solar-induced chlorophyll fluorescence.

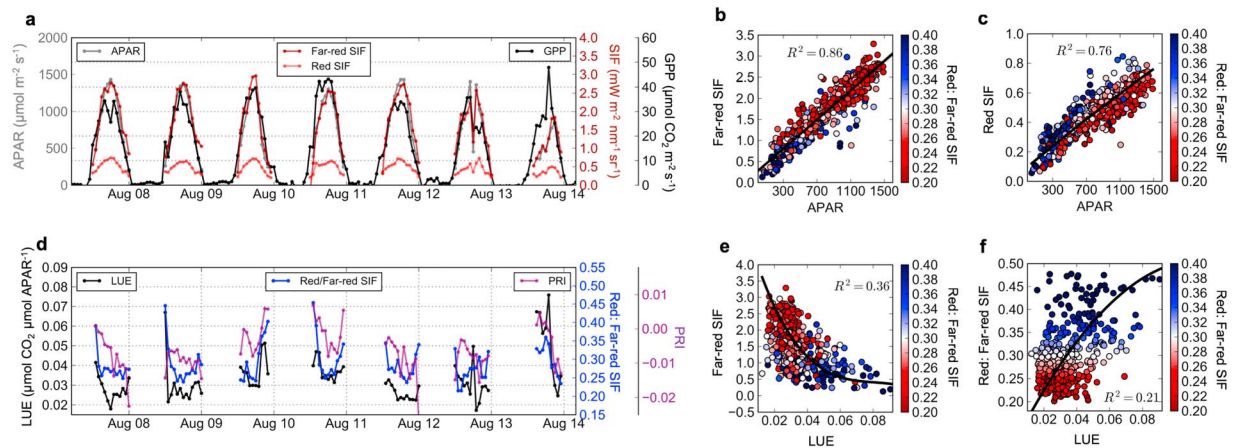


Figure 6. Diurnal dynamics of mean hourly red SIF, far-red SIF, gross primary production (GPP), absorbed photosynthetically active radiation (APAR), light-use efficiency (LUE), red:far-red SIF, and photochemical reflectance index (PRI) as observed from a canopy spectrometer in soybean. (a) Mean hourly data for APAR (gray), GPP (black), far-red SIF (dark red), and red SIF (light red) during a 7-day period from 7 to 14 August 2017. (b) Mean hourly APAR against mean hourly far-red SIF during peak greenness (when little change in red:far-red SIF occurs), colored dots represent the daily mean red:far-red ratio. (c) Same as (b) except with red SIF. (d) Mean hourly data for LUE (black); red:far-red SIF (blue), and PRI (purple). (e) Relationship between hourly LUE and far-red SIF colored by red:far-red SIF during peak greenness. (f) Same as (e) except with red:far-red SIF. SIF = solar-induced chlorophyll fluorescence.

driven by APAR. Similarly, PRI also corresponds with changes in LUE with similar statistical power ($R^2 = 0.21$, $p < 0.05$).

3.6. The Red:Far-Red ChlF Ratio and Photosynthesis

Due to the fact that current remote sensing instruments are not capable of retrieving the full ChlF spectrum and can only measure emitted photons within narrow atmospheric windows (i.e., regions of isolated solar Fraunhofer lines, or oxygen A and B bands), we investigate changes in leaf red:far-red $F_{t,\lambda}$ across two distinct wavelength regions identical to those retrieved from our canopy spectrometer (red = 680–686 nm, far-red = 745–758 nm). As such, we compare changes in the red:far-red ChlF ratio during complete light response curves within individual species against photosynthesis for *G. max* (soybean) leaves grown under low (circles), moderate (squares), and high (triangles) water stress conditions (Figure 7a). A systematic decrease in ChlF magnitude across the entire spectral range is found at equivalent light levels driven by the downregulation of photosynthesis and increase in NPQ. The change in red:far-red ($\Delta F_{t,\text{red}}/F_{t,\text{far-red}}$) within individual leaves approaches 15% for highly stressed leaves, and about 5% for unstressed leaves. Meanwhile, a decrease in the magnitude of $F_{t,740}$ (where minimal shape changes occur) of around 40% and a decrease in net photosynthesis of around 75% is found (Figure 7a).

At the canopy scale during peak greenness (25 July to 5 September), a close correspondence between hourly far-red SIF and GPP is found (Figure 7b), albeit weaker than that with APAR (Figure 6). During this time we expect little day-to-day variation in red:far-red SIF, but posit that diurnal variation in this ratio could be due to photosynthetic downregulation. However, this is not made obvious by Figure 7b, and a multiple linear regression using both far-red and red SIF to predict GPP only slightly improves the R^2 to 0.55—suggesting that there is limited additive information in the red:far-red SIF ratio for improving predictions of GPP. This does not rule out the potential that red:far-red SIF will likely be more strongly correlated with LUE at a site with a greater range of stress than that observed here. Additionally, we observed a shift from a nonlinear to linear model when scaling the fluorescence/photosynthesis relationship from the leaf to the canopy (Figure 7). An explanation for this is likely due to spatial and temporal averaging, whereby as more leaves (and thus leaf angles) are averaged within a larger footprint, the integrated canopy effective APAR is reduced, limiting the high saturation potential of canopy SIF and GPP. Complex scaling issues such as this have been addressed by modeling communities by separating canopies into sunlit and shaded portions or vertically integrating against a radiation gradient, for example (Chen et al., 1999). Building on this, a quantitatively rigorous explanation is required to explain scaling phenomena as they relate to SIF and photosynthesis, some of which have been explored (Liu et al., 2018; Porcar-Castell et al., 2014; Romero et al., 2017; van Wittenberghe et al., 2015).

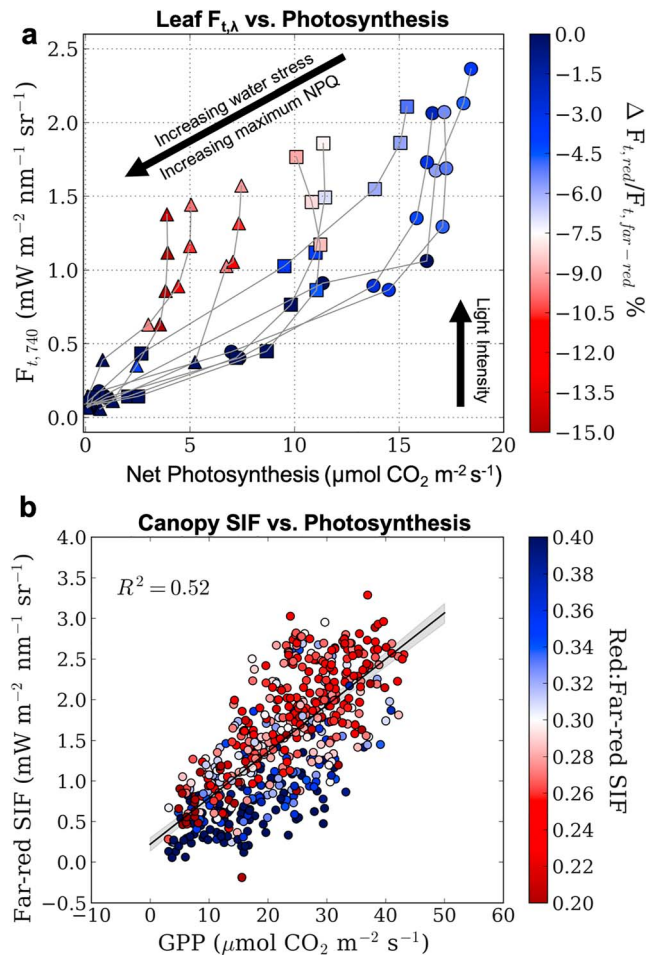


Figure 7. Relationships of leaf and canopy far-red fluorescence with photosynthesis. (a) Individual light response curves ($n = 9$) are indicated by the gray lines connecting measurements made at increasing light levels (50–1,500 PAR). Triangles indicate *G. max* plants under high levels of water stress, square represent moderate stress, and circles indicate no water stress. The change in red:far-red $F_{t,\lambda}$ represents the percent change of each individual sample exposed to each subsequent increase in light intensity. (b) Relationship between hourly far-red SIF and GPP during peak greenness at the canopy scale, colored by red:far-red ratio. SIF = solar-induced chlorophyll fluorescence.

4. Discussion

From this work, several findings have implications for remote sensing of the SIF spectral shape: (1) across a wide range of species, ~85% of the spectral variance in ChlF can be explained by changes in the magnitude of a mean spectral shape. This implies that the spectral shape is quite stable and that all wavelength ranges respond to changes in variable PSII fluorescence yield driven by PQ and NPQ; (2) far-red SIF is more closely correlated to photosynthesis and APAR than red SIF (Figures 5–7), because it is less prone to re-absorption by Chl at both leaf and canopy scales (Fournier et al., 2012; Yang & van der Tol, 2018). At the canopy scale, the strong correlation between SIF and APAR (Figures 5 and 6) confirms previous results in crop canopies (Miao et al., 2018; Yang et al., 2018), which makes intuitive sense since APAR covaries with seasonal changes in leaf area in these systems, and is prone to less error than calculated GPP fluxes; and (3) Since wavelengths in the far-red spectrum are less impacted by confounding factors such as chlorophyll or canopy structure (Figure S12), current satellite retrievals in this region may be better suited to assess stress induced downregulation of photosynthesis than changes in the ChlF spectral shape alone.

Our results support a large body of research suggesting that deviations from the mean spectral shape of ChlF are mostly controlled by chlorophyll concentration, which regulates the degree of reabsorption in the red part of the spectrum along the photon escape path (Buschmann, 2007; Gitelson et al., 1998; Lichtenthaler et al., 1990). As such, two wavelengths alone may be sufficient to pinpoint the primary variance in steady-state ChlF spectra (Figures 1c and 3c), that is, 685 and 750 nm. However, these wavelengths are also confounded by overlapping spectral changes associated with NPQ, albeit to a lesser extent (Figures 1e, 3e, and 4d). At the leaf scale, we show that the spectrally integrated spectrum is only modulated by 8% through the reabsorption of emitted ChlF, but by up to about 20% in the red region (Figure 1c); notably, the spectral and sample weights would be significantly amplified for highly chlorotic leaves, which are not included in this study. However, at the canopy scale, we do observe an amplification of the red:far-red SIF ratio during senescence (Figure 5d) because more red photons are prone to escape the canopy when leaves become highly chlorotic (Figures S9 and S10; Fournier et al., 2012; Goulas et al., 2017; Yang & van der Tol, 2018). Further, while we attribute PC2 at steady-state changes primarily to chlorophyll concentration, confounding effects of leaf-level radiative transfer should not be

negated. Variance in the spectral shape of leaf-level ChlF is likely also impacted by structural parameters not measured by this study, including but not limited to cell arrangement, mesophyll structure, leaf thickness, and chloroplast movement. Future research should focus on the impacts of these components on leaf-level radiative transfer, and our interpretation of bidirectional SIF emission (van Wittenberghe et al., 2015).

In our analysis, we have to distinguish between two different effects controlled by NPQ dynamics: (1) NPQ decreases the overall fluorescence yield, leading to a reduction in the overall magnitude of fluorescence across all wavelengths (e.g., see Figures 4 and 7), even at 850 nm (Joiner et al., 2012), where ChlF can be measured from space; and (2) NPQ drives small changes in the spectral shape of ChlF. The challenge of using absolute magnitude changes as a stress indicator from space is to disentangle these from changes in APAR (driven by chlorophyll and leaf area). Research suggests that changes in the spectral shape might help, but we find that these changes impose high requirements on measurement accuracy from space and a sound quantitative understanding of radiative transfer. Rather, information on the red:far-red SIF ratio, or vegetation reflectance data, could be used to decouple the dominant APAR impact on the SIF magnitude (Yang & van der Tol, 2018).

In the deviations from the average spectral shape, we find a ChlF decrease at 680 nm, an increase at 720 nm, and a smaller decrease around 760 nm associated with increased NPQ (PC3 in Figures 1 and 3; PC2 in Figure 4) are related to changes in the relative contribution of PSI and PSII ChlF. In our comparison of individual leaves across a diverse range of species (Figure 1), we show that—to third order—the shape of the spectrum varies similarly to the primary variance associated with NPQ dynamics during changes in illumination condition (Figures 4d and 4e) and rapid photosynthetic induction (Figures S7 and S8). While the empirical relationship between PC3 and NPQ in this experiment is weak but slightly positive (Figure 1f), it could be explained by the relatively small influence PC3 has on the overall spectra under conditions where APAR and Chl concentration vary strongly. Another explanation is that NPQ relaxation kinetics in this context are associated primarily with the slow phases of relaxation, whereas the light-response curve experiments examine the rapid or middle phases of relaxation (Horton & Hague, 1988; Quick & Stitt, 1989). Additionally, if leaves with higher rates of sustained NPQ (more stressed) were included in this study we would expect to see a larger variation in PC3 in Figure 1, and a greater change in ChlF magnitude. The NPQ related spectral shape shift would also be greater if primarily sun-exposed leaves, which are known to have higher xanthophyll cycle pools and NPQ rates (Magney, Logan, et al., 2017; Niinemets, 2007), were sampled. Nonetheless, it is remarkable that even at steady state, the SVD analysis is able to capture a tertiary component of variance, despite the relatively small influence this has on the overall spectrum.

The spectral shape associated with changes in NPQ shows a similar pattern to Farooq et al. (2018) and Lambrev et al. (2010), suggesting that the change at $F_{t,720}$ is the result of rapidly reversible energy-dependent quenching, whereas the decrease at $F_{t,680}$ is induced by both PsbS-independent mechanisms and energy-dependent quenching. Further, the decrease in $F_{t,680}$ under increasing light has been noted in other works and attributed to changes in PSII compared to PSI fluorescence (Nematov et al., 2017), since PSI fluorescence is thought to be negligible <680 nm and not modified by changes in NPQ/PQ (Franck et al., 2002; Palombi et al., 2011; Figures S7 and S8). Indeed, our canopy results show a decrease in red:far-red SIF with increasing light and changes in LUE (Figures 6 and S12); however, even under highly stressed conditions (Figure 7), the leaf level change in red:far-red ChlF is only 15%, which would require a significant improvement in SIF retrievals (which currently have systematic errors of the same or greater magnitude) to utilize red:far-red SIF to assess NPQ dynamics.

The range of experiments presented is somewhat analogous to how different remote sensing platforms may observe canopies at shorter (diurnal) and longer timescales (seasonal). At the canopy scale, some studies have indicated that red:far-red SIF can vary by over 50% during the course of a day, suggesting that this is a dynamic diurnal response of plants to environmental stress (Cheng et al., 2013; Middleton et al., 2017; Rossini et al., 2016; Wieneke et al., 2016, 2018). Based on our leaf and canopy measurements, we consider that preferential quenching of PSII alone is unlikely to explain this variation, even for highly stressed leaves (Figures 3 and 7). However, a notably smaller range of stress (and higher photosynthetic capacity) is experienced for our canopy data in this agricultural setting compared to traditional field conditions. Nonetheless, a systematic decrease in far-red fluorescence magnitude corresponds to changes in photosynthesis at both leaf and canopy scales to a greater extent than changes in red:far-red ChlF in these experiments (Figures 6 and 7). While the change in red:far-red ChlF at both leaf and canopy scales associated with photosynthetic downregulation is encouraging, it is likely more practical to use the red:far-red ratio to infer changes in canopy structure or Chl from satellite platforms.

5. Conclusions

Here, a comprehensive statistical analysis of *where*, *why*, and *to what extent* leaf-scale ChlF emission spectra change across a diverse range of species and conditions is used to interpret SIF at the canopy scale. We show that red:far-red canopy SIF is largely controlled by canopy structure (leaf area) and chlorophyll at the seasonal timescale, and that a decrease in red:far-red SIF at shorter timescales (diurnal) is comparable to changes in leaf-level red:far-red $F_{t,\lambda}$ —potentially due to diurnal dynamics in NPQ or photosynthetic downregulation. However, variations in the ratio that exceed 10–15% should not be attributed to changes solely in PSI and PSII contributions due to dynamic photosynthetic downregulation. Rather, photosynthetic downregulation more aptly corresponds to decreases in the fluorescence magnitude across the entire spectrum. Future work could use the red:far-red ratio to decouple the impact of chlorophyll and canopy

structure on changes in fluorescence magnitude, which in turn could be used to assess rapid changes in plant photosynthesis.

While the core focus of our work is on the leaf-scale, future research at flux tower sites linking canopy red and far-red SIF (or retrievals from other wavelength windows) to photosynthesis across diverse ecosystems and environmental stressors is warranted. If global retrievals of SIF are to estimate photosynthetic downregulation from changes in the spectral shape alone, a significant reduction in SIF retrieval noise accompanied with high temporal resolutions (i.e., geostationary orbit) will be necessary to detect the small effect of NPQ on red:far-red ChlF dynamics. Even more importantly, small systematic biases can alias into the red:far-red ratio and will need to be kept well below 5%, which is a rather stringent requirement. It remains important for the remote sensing community to understand the fundamental factors influencing changes in the spectral shape of ChlF at multiple scales, and the incorporation of this understanding in radiative transfer models, to fully interpret what we can observe from current and future remote sensing platforms.

Acknowledgments

We thank Madeline Gillman, Anu Riikonen, and Paulina Rajewicz for help with data collection; Ari Kornfeld, and Katharina Seibt for insightful suggestions on the instrumental setup, experimental design and interpretation of analysis; the Huntington Library for access to laboratory space and the botanical collection; La Selva Biological Research Station; Hyytiälä Forestry Field Station; and Forrest Goodman, among others, from the National Laboratory for Agriculture and the Environment (USDA-ARS) in Ames, Iowa, for infrastructure and institutional support. The research was supported by a NASA Postdoctoral Program Fellowship and INTERACT transnational access (TA) under the European Union H2020 Grant Agreement 730938 to T. S. M., California Institute of Technology startup funds to C. F., NASA IDS support to J. B. F., Academy of Finland (grants 288039 and 293443) support to A. P.-C., the Keck Institute for Space Studies, and the NASA Carbon Cycle Science program (16-CARBON16-0119). The research was carried out, in part, at the Jet Propulsion Laboratory, California Institute of Technology, under a contract with the National Aeronautics and Space Administration. California Institute of Technology. Government sponsorship acknowledged. We declare no conflict of interest. The data sets used to prepare the figures for the current study are available at data repository hosted at the California Institute of Technology (<https://data.caltech.edu/records/1226>). The doi associated with this data set is 10.22002/D1.1226. Please contact the authors if you plan to use the data.

References

- Ač, A., Malenovský, Z., Olejníčková, J., Gallé, A., Rascher, U., & Mohammed, G. (2015). Meta-analysis assessing potential of steady-state chlorophyll fluorescence for remote sensing detection of plant water, temperature and nitrogen stress. *Remote Sensing of Environment*, *168*, 420–436. <https://doi.org/10.1016/j.rse.2015.07.022>
- Agati, G. (1998). Response of the in vivo chlorophyll fluorescence spectrum to environmental factors and laser excitation wavelength A portable fibre-probe UV LED-induced fluorescence detection system Response of the in vivo chlorophyll fluorescence spectrum to environment. *Pure and Applied Physics*, *7*, 979–807.
- Atherton, J., Olascoaga, B., Alonso, L., & Porcar-Castell, A. (2017). Spatial variation of leaf optical properties in a boreal forest is influenced by species and light environment. *Frontiers in Plant Science*, *8*, 309. <https://doi.org/10.3389/fpls.2017.00309>
- Baker, N. R. (2008). Chlorophyll fluorescence: A probe of photosynthesis in vivo. *Annual Review of Plant Biology*, *59*(1), 89–113. <https://doi.org/10.1146/annurev.arplant.59.032607.092759>
- Buschmann, C. (2007). Variability and application of the chlorophyll fluorescence emission ratio red/far-red of leaves. *Photosynthesis Research*, *92*(2), 261–271. <https://doi.org/10.1007/s11120-007-9187-8>
- Carter, G. A., Theisen, A. F., & Mitchell, R. J. (1990). Chlorophyll fluorescence measured using the Fraunhofer line-depth principle and relationship to photosynthetic rate in the field. *Plant, Cell & Environment*, *13*(1), 79–83. <https://doi.org/10.1111/j.1365-3040.1990.tb01302.x>
- Chen, J., Liu, J., Cihlar, J., & Goulden, M. (1999). Daily canopy photosynthesis model through temporal and spatial scaling for remote sensing applications. *Ecological Modelling*, *124*(2–3), 99–119. [https://doi.org/10.1016/s0304-3800\(99\)00156-8](https://doi.org/10.1016/s0304-3800(99)00156-8)
- Cheng, Y.-B., Middleton, E., Zhang, Q., Huemmrich, K., Campbell, P., Corp, L., et al. (2013). Integrating solar induced fluorescence and the photochemical reflectance index for estimating gross primary production in a cornfield. *Remote Sensing*, *5*(12), 6857–6879. <https://doi.org/10.3390/rs5126857>
- Croce, R., Zucchelli, G., Garlaschi, F., Bassi, R., & Jennings, R. (1996). Excited state equilibration in the photosystem light-harvesting-complex: P700 is almost isoenergetic with its antenna. *Biochemistry*, *35*(26), 8572–8579. <https://doi.org/10.1021/bi960214m>
- Datt, B. (1999). A new reflectance index for remote sensing of chlorophyll content in higher plants: Tests using Eucalyptus leaves. *Journal of Plant Physiology*, *154*(1), 30–36. [https://doi.org/10.1016/S0176-1617\(99\)80314-9](https://doi.org/10.1016/S0176-1617(99)80314-9)
- Davis, T. S., Bosque-Pérez, N. A., Foote, N. E., Magney, T., & Eigenbrode, S. D. (2015). Environmentally dependent host-pathogen and vector-pathogen interactions in the Barley yellow dwarf virus pathosystem. *Journal of Applied Ecology*, *52*(5), 1392–1401. <https://doi.org/10.1111/1365-2664.12484>
- Dold, C., Hatfield, J. L., Prueger, J. H., Sauer, T. J., Moorman, T. B., & Wacha, K. M. (2019). Impact of management practices on carbon and water fluxes in corn—Soybean rotations. *Agrosystems, Geosciences, & Environment*, *2*(1), 1–8. <https://doi.org/10.2134/age2018.08.0032>
- Drusch, M., Moreno, J., del Bello, U., Franco, R., Goulas, Y., Huth, A., et al. (2016). The Fluorescence EXplorer Mission Concept—ESA's Earth Explorer 8. *IEEE Transactions on Geoscience and Remote Sensing*, *55*(3), 1273–1284. <https://doi.org/10.1109/TGRS.2016.2621820>
- Farooq, S., Chmeliov, J., Wientjes, E., Koehorst, R., Bader, A., Valkunas, L., et al. (2018). Dynamic feedback of the photosystem II reaction centre on photoprotection in plants. *Nature Plants*, *4*(4), 225–231. <https://doi.org/10.1038/s41477-018-0127-8>
- Fournier, A., Daumard, F., Champagne, S., Ounis, A., Goulas, Y., & Moya, I. (2012). Effect of canopy structure on sun-induced chlorophyll fluorescence. *ISPRS Journal of Photogrammetry and Remote Sensing*, *68*(120), 112–120. <https://doi.org/10.1016/j.isprsjprs.2012.01.003>
- Franck, F., Dewez, D., & Popovic, R. (2005). Changes in the room-temperature emission spectrum of chlorophyll during fast and slow phases of the Kautsky effect in intact leaves. *Photochemistry and Photobiology*, *81*(2), 431–436. <https://doi.org/10.1562/2004-03-01-RA-094>
- Franck, F., Juneau, P., & Popovic, R. (2002). Resolution of the Photosystem I and Photosystem II contributions to chlorophyll fluorescence of intact leaves at room temperature. *Biochimica et Biophysica Acta - Bioenergetics*, *1556*(2–3), 239–246. [https://doi.org/10.1016/S0005-2728\(02\)00366-3](https://doi.org/10.1016/S0005-2728(02)00366-3)
- Frankenberg, C., Fisher, J. B., Worden, J., Badgley, G., Saatchi, S. S., Lee, J.-E., et al. (2011). New global observations of the terrestrial carbon cycle from GOSAT: Patterns of plant fluorescence with gross primary productivity. *Geophysical Research Letters*, *38*, L17706. <https://doi.org/10.1029/2011GL048738>
- Fraunhofer, J. (1817). Bestimmung des Brechungs- und des Farbenzerstreuungs-Vermögens verschiedener Glasarten, in Bezug auf die Vervollkommnung achromatischer Fernrohre. *Annals of Physics*, *56*(7), 264–313. <https://doi.org/10.1002/andp.18170560706>
- Gamon, J. A., Penuelas, J., & Field, C. B. (1992). A narrow-waveband spectral index that tracks diurnal changes in photosynthetic efficiency. *Remote Sensing of Environment*, *41*(1), 35–44. [https://doi.org/10.1016/0034-4257\(92\)90059-S](https://doi.org/10.1016/0034-4257(92)90059-S)
- Garbulsky, M. F., Peñuelas, J., Gamon, J., Inoue, Y., & Filella, I. (2011). The photochemical reflectance index (PRI) and the remote sensing of leaf, canopy and ecosystem radiation use efficiencies: A review and meta-analysis. *Remote Sensing of Environment*, *115*(2), 281–297. <https://doi.org/10.1016/j.rse.2010.08.023>

- Genty, B., Wonders, J., & Baker, N. R. (1990). Non-photochemical quenching of Fo in leaves is emission wavelength dependent: consequences for quenching analysis and its interpretation. *Photosynthesis Research*, 26(133), 133–139.
- Gitelson, A. A., Buschmann, C., & Lichtenthaler, H. K. (1998). Leaf chlorophyll fluorescence corrected for re-absorption by means of absorption and reflectance measurements. *Journal of Plant Physiology*, 152(2–3), 283–296. [https://doi.org/10.1016/S0176-1617\(98\)80143-0](https://doi.org/10.1016/S0176-1617(98)80143-0)
- Goulas, Y., Fournier, A., Daumard, F., Champagne, S., Ounis, A., Marloie, O., & Moya, I. (2017). Gross primary production of a wheat canopy relates stronger to far red than to red solar-induced chlorophyll fluorescence. *Remote Sensing*, 9(1), 97. <https://doi.org/10.3390/rs9010097>
- Grossmann, K., Frankenberg, C., Magney, T. S., Herlock, S., Siebt, U., & Stutz, J. (2018). PhotoSpec: A new instrument to measure spatially distributed red and far-red solar induced chlorophyll fluorescence. *Remote Sensing of Environment*, 216, 311–327. <https://doi.org/10.1016/j.rse.2018.07.002>
- Guanter, L., Zhang, Y., Jung, M., Joiner, J., Voigt, M., Berry, J. A., et al. (2014). Global and time-resolved monitoring of crop photosynthesis with chlorophyll fluorescence. *Proceedings of the National Academy of Sciences of the United States of America*, 111(14), E1327–E1333. <https://doi.org/10.1073/pnas.132008111>
- Hak, R., Lichtenthaler, H. K., & Rinderle, U. (1990). Decrease of the chlorophyll fluorescence ratio F690/F730 during greening and development of leaves. *Radiation and Environmental Biophysics*, 29(4), 329–336. <https://doi.org/10.1007/BF01210413>
- Hasegawa, M., Shiina, T., Terazima, M., & Kumazaki, S. (2010). Selective excitation of photosystems in chloroplasts inside plant leaves observed by near-infrared laser-based fluorescence spectral microscopy. *Plant and Cell Physiology*, 51(2), 225–238. <https://doi.org/10.1093/pcp/pcp182>
- Horton, P., & Hague, A. (1988). Studies on the induction of chlorophyll fluorescence quenching in isolated barley chloroplasts. IV. Resolution of nonphotochemical quenching. *Biochimica et Biophysica Acta*, 932, 107–115. [https://doi.org/10.1016/0005-2728\(88\)90144-2](https://doi.org/10.1016/0005-2728(88)90144-2)
- Johnson, D. M., Smith, W. K., Vogelmann, T. C., & Brodersen, C. R. (2005). Leaf architecture and direction of incident light influence mesophyll fluorescence profiles. *American Journal of Botany*, 92(9), 1425–1431. <https://doi.org/10.3732/ajb.92.9.1425>
- Joiner, J., Yoshida, Y., Guanter, L., & Middleton, E. M. (2016). New methods for retrieval of chlorophyll red fluorescence from hyperspectral satellite instruments: simulations and application to GOME-2 and SCIAMACHY. *Atmospheric Measurement Techniques Discussions*, 1–41. <https://doi.org/10.5194/amt-2015-387>
- Joiner, J., Yoshida, Y., Vasilkov, A., Middleton, E., Campbell, P., & Kuze, A. (2012). Filling-in of near-infrared solar lines by terrestrial fluorescence and other geophysical effects: simulations and space-based observations from SCIAMACHY and GOSAT. *Atmospheric Measurement Techniques*, 5(4), 809–829. <https://doi.org/10.5194/amt-5-809-2012>
- Joiner, J., Yoshida, Y., Vasilkov, A. P., Corp, L. A., & Middleton, E. M. (2011). First observations of global and seasonal terrestrial chlorophyll fluorescence from space. *Biogeosciences*, 8(3), 637–651. <https://doi.org/10.5194/bg-8-637-2011>
- Kautsky, H., & Hirsch, A. (1931). Neue Versuche zur Kohlensäureassimilation. *Naturwissenschaften*, 19(48), 964. <https://doi.org/10.1007/BF01516164>
- Kitajima, K., & Butler, W. L. (1975). Quenching of chlorophyll fluorescence and primary photochemistry in chloroplasts by dibromothymoquinone. *Biochimica et Biophysica Acta (BBA) - Bioenergetics*, 376(1), 105–115. [https://doi.org/10.1016/0005-2728\(75\)90209-1](https://doi.org/10.1016/0005-2728(75)90209-1)
- Krause, G., & Weis, E. (1991). Chlorophyll fluorescence and photosynthesis: the basics. *Annual Review of Plant Biology*, 42(1), 313–349. <https://doi.org/10.1146/annurev.pp.42.060191.001525>
- Lambrev, P. H., Nilkens, M., Miloslavina, Y., Jahns, P., & Holzwarth, A. R. (2010). Kinetic and spectral resolution of multiple nonphotochemical quenching components in Arabidopsis leaves. *Plant Physiology*, 152(3), 1611–1624. <https://doi.org/10.1104/pp.109.148213>
- Lazar, D. (1999). Chlorophyll a fluorescence induction. *Biochimica et Biophysica Acta*, 1412, 1–28.
- Lichtenthaler, H. K., Hak, R., & Rinderle, U. (1990). The chlorophyll fluorescence ratio F690/F730 in leaves of different chlorophyll content. *Photosynthesis Research*, 25(3), 295–298. <https://doi.org/10.1007/BF00033170>
- Lichtenthaler, H. K., Wenzel, O., Buschmann, C., & Gitelson, A. (1998). Plant Stress Detection by Reflectance and Fluorescence. *Annals of the New York Academy of Sciences*, 851(1), 271–285. <https://doi.org/10.1111/j.1749-6632.1998.tb09002.x>
- Liu, X., Guanter, L., Liu, L., Damm, A., Malenovsky, Z., Rascher, U., et al. (2018). Downscaling of solar-induced chlorophyll fluorescence from canopy level to photosystem level using a random forest model. *Remote Sensing of Environment*, (9). <https://doi.org/10.1016/j.rse.2018.05.035>
- Magney, T. S., Frankenberg, C., Fisher, J. B., Sun, Y., North, G. B., Davis, T. S., et al. (2017). Connecting active to passive fluorescence with photosynthesis: A method for evaluating remote sensing measurements of Chl fluorescence. *New Phytologist*, 215(4), 1594–1608. <https://doi.org/10.1111/nph.14662>
- Magney, T. S., Logan, B. A., Reblin, J. S., Boelman, N. T., Eitel, J. U. H., Greaves, H. E., et al. (2017). Xanthophyll Cycle Activity in Two Prominent Arctic Shrub Species. *Arctic, Antarctic, and Alpine Research*, 49(2), 277–289. <https://doi.org/10.1657/AAAR0016-044>
- Magney, T. S., Bowling, D. R., Logan, B., Grossmann, K., Stutz, J., Blanken, P., et al. (2019). Mechanistic evidence for tracking the seasonality of photosynthesis with solar-induced fluorescence. *Proceedings of the National Academy of Sciences*. <https://doi.org/10.1073/pnas.1900278116>
- Magney, T. S., Vierling, L. A., Eitel, J. U. H., Huggins, D. R., & Garrity, S. R. (2016). Response of high frequency Photochemical Reflectance Index (PRI) measurements to environmental conditions in wheat. *Remote Sensing of Environment*, 173, 84–97. <https://doi.org/10.1016/j.rse.2015.11.013>
- Meroni, M., Rossini, M., Guanter, L., Alonso, L., Rascher, U., Colombo, R., & Moreno, J. (2009). Remote sensing of solar-induced chlorophyll fluorescence: Review of methods and applications. *Remote Sensing of Environment*, 113(10), 2037–2051. <https://doi.org/10.1016/j.rse.2009.05.003>
- Miao, G., Guan, K., Yang, X., Bernacchi, C. J., Berry, J. A., DeLucia, E. H., et al. (2018). Sun-Induced Chlorophyll Fluorescence, Photosynthesis, and Light Use Efficiency of a Soybean Field. *Journal of Geophysical Research: Biogeosciences*, 610–623. <https://doi.org/10.1002/2017JG004180>
- Middleton, E. M., Rascher, U., Corp, L. A., Huemmrich, K. F., Cook, B. D., Noormets, A., et al. (2017). The 2013 FLEX—US Airborne Campaign at the Parker Tract Loblolly Pine Plantation in North Carolina, USA. *Remote Sensing*, 9(6), 1–31. <https://doi.org/10.3390/rs9060612>
- Nematov, S., Paola, A., Remelli, W., Khuvondikov, V., & Santabarbara, S. (2017). BBA—Bioenergetics Spectral dependence of irreversible light-induced fluorescence quenching: Chlorophyll forms with maximal emission at 700 – 702 and 705 – 710 nm as spectroscopic

- markers of conformational changes in the core complex. *BBA - Bioenergetics*, 1858(7), 529–543. <https://doi.org/10.1016/j.bbabi.2017.05.002>
- Niinemets, U. (2007). Photosynthesis and resource distribution through plant canopies. *Plant, Cell & Environment*, 30(9), 1052–1071. <https://doi.org/10.1111/j.1365-3040.2007.01683.x>
- Palombi, L., Cecchi, G., Lognoli, D., Raimondi, V., Toci, G., & Agati, G. (2011). A retrieval algorithm to evaluate the Photosystem I and Photosystem II spectral contributions to leaf chlorophyll fluorescence at physiological temperatures. *Photosynthesis Research*, 108(2–3), 225–239. <https://doi.org/10.1007/s11120-011-9678-5>
- Parry, C., Blonquist, M. J., & Bugbee, B. (2014). In situ measurement of leaf chlorophyll concentration: analysis of the optical/absolute relationship. *Plant, Cell & Environment*, 37(11), 2508–2520. <https://doi.org/10.1111/pce.12324>
- Pinto, F., Damm, A., Schickling, A., Panigada, C., Cogliati, S., Müller-Linow, M., et al. (2016). Sun-induced chlorophyll fluorescence from high-resolution imaging spectroscopy data to quantify spatio-temporal patterns of photosynthetic function in crop canopies. *Plant, Cell & Environment*, 39(7), 1500–1512. <https://doi.org/10.1111/pce.12710>
- Plascyk, J. A., & Gabriel, F. C. (1975). The Fraunhofer line discriminator MKII an airborne instrument for precise and standardized ecological luminescence measurement. *IEEE Transactions on Instrumentation and Measurement*, 24(4), 306–313. <https://doi.org/10.1109/TIM.1975.4314448>
- Platt, U., & Stutz, J. (2008). *Differential Optical Absorption Spectroscopy: Principles and Applications*. Berlin Heidelberg: Springer.
- Porcar-Castell, A., Tyystjärvi, E., Atherton, J., van der Tol, C., Flexas, J., Pfündel, E. E., et al. (2014). Linking chlorophyll a fluorescence to photosynthesis for remote sensing applications: mechanisms and challenges. *Journal of Experimental Botany*, 65(15), 4065–4095. <https://doi.org/10.1093/jxb/eru191>
- Quick, P., & Stitt, M. (1989). An examination of factors contributing to non-photochemical quenching of chlorophyll fluorescence in barley leaves. *Biochimica et Biophysica Acta (BBA) - Bioenergetics*, 977(3), 287–296. [https://doi.org/10.1016/S0005-2728\(89\)80082-9](https://doi.org/10.1016/S0005-2728(89)80082-9)
- Rajewicz, P. A., Atherton, J., & Alonso, L. (2019). Leaf-level spectral fluorescence measurements: Comparing methodologies for broad-leaves and needles. *Remote Sensing*, 11(5), 532. <https://doi.org/10.3390/rs11050532>
- Rascher, U., Alonso, L., Burkart, A., Cilia, C., Cogliati, S., Colombo, R., et al. (2015). Sun-induced fluorescence—A new probe of photosynthesis: First maps from the imaging spectrometer HyPlant. *Global Change Biology*, 21(12), 4673–4684. <https://doi.org/10.1111/gcb.13017>
- Reichstein, M., Subke, J.-A., Angeli, A. C., & Tenhunen, J. D. (2005). Does the temperature sensitivity of decomposition of soil organic matter depend upon water content, soil horizon or incubation time.pdf. *Global Change Biology*, 11, 1754–1767. <https://doi.org/10.1111/j.1365-2486.2005.01010.x>
- Rizzo, F., Zucchelli, G., Jennings, R., & Santabarbara, S. (2014). Wavelength dependence of the fluorescence emission under conditions of open and closed Photosystem II reaction centres in the green alga *Chlorella sorokiniana*. *Biochimica et Biophysica Acta - Bioenergetics*, 1837(6), 726–733. <https://doi.org/10.1016/j.bbabi.2014.02.009>
- Romero, J. M., Cordon, G. B., & Lagorio, M. G. (2017). Modeling re-absorption of fluorescence from the leaf to the canopy level. *Remote Sensing of Environment*, 204, 138–146. <https://doi.org/10.1016/j.rse.2017.10.035>
- Rossini, M., Meroni, M., Celesti, M., Cogliati, S., Julitta, T., Panigada, C., et al. (2016). Analysis of red and far-red Sun-induced chlorophyll fluorescence and their ratio in different canopies based on observed and modeled data. *Remote Sensing*, 8(5), 412–428. <https://doi.org/10.3390/rs8050412>
- Schimel, D., Pavlick, R., Fisher, J. B., Asner, G. P., Saatchi, S., Townsend, P., et al. (2015). Observing terrestrial ecosystems and the carbon cycle from space. *Global Change Biology*, 21(5), 1762–1776. <https://doi.org/10.1111/gcb.12822>
- Schreiber, U., Schliwa, U., & Bilger, W. (1986). Continuous recording of photochemical and non-photochemical chlorophyll fluorescence quenching with a new type of modulation fluorometer. *Photosynthesis Research*, 10(1–2), 51–62. <https://doi.org/10.1007/BF00024185>
- Stirbet, A., & Govindjee (2011). On the relation between the Kautsky effect (chlorophyll a fluorescence induction) and Photosystem II: Basics and applications of the OJIP fluorescence transient. *Journal of Photochemistry and Photobiology B: Biology*, 104(1–2), 236–257. <https://doi.org/10.1016/j.jphotobiol.2010.12.010>
- Sun, Y., Frankenberg, C., Jung, M., Joiner, J., Guanter, L., Köhler, P., & Magney, T. (2018). Overview of Solar-Induced chlorophyll Fluorescence (SIF) from the Orbiting Carbon Observatory-2: Retrieval, cross-mission comparison, and global monitoring for GPP. *Remote Sensing of Environment*, 209, 808–823. <https://doi.org/10.1016/j.rse.2018.02.016>
- Sun, Y., Frankenberg, C., Wood, J. D., Schimel, D. S., Jung, M., Guanter, L., et al. (2017). OCO-2 advances photosynthesis observation from space via solar-induced chlorophyll fluorescence. *Science*, 358(6360), eaam5747. <https://doi.org/10.1126/science.aam5747>
- van der Tol, C., Berry, J. A., Campbell, P., & Rascher, U. (2014). Models of fluorescence and photosynthesis for interpreting measurements of solar-induced chlorophyll fluorescence. *Journal of Geophysical Research: Biogeosciences*, 119, 2312–2327. <https://doi.org/10.1002/2014JG002713>
- van der Tol, C., Verhoef, W., & Rosema, A. (2009). A model for chlorophyll fluorescence and photosynthesis at leaf scale. *Agricultural and Forest Meteorology*, 149(1), 96–105. <https://doi.org/10.1016/j.agrformet.2008.07.007>
- van der Tol, C., Verhoef, W., Timmermans, J., Verhoef, a., & Su, Z. (2009). An integrated model of soil-canopy spectral radiances, photosynthesis, fluorescence, temperature and energy balance. *Biogeosciences*, 6(12), 3109–3129. <https://doi.org/10.5194/bg-6-3109-2009>
- Vilfan, N., van der Tol, C., Müller, O., Rascher, U., & Verhoef, W. (2016). Fluspect-B: A model for leaf fluorescence, reflectance and transmittance spectra. *Remote Sensing of Environment*, 186, 596–615. <https://doi.org/10.1016/j.rse.2016.09.017>
- Wieneke, S., Ahrends, H., Damm, A., Pinto, F., Stadler, A., Rossini, M., & Rascher, U. (2016). Airborne based spectroscopy of red and far-red sun-induced chlorophyll fluorescence: Implications for improved estimates of gross primary productivity. *Remote Sensing of Environment*, 184, 654–667. <https://doi.org/10.1016/j.rse.2016.07.025>
- Wieneke, S., Burkart, A., Cendrero-Mateo, M. P., Julitta, T., Rossini, M., Schickling, A., et al. (2018). Linking photosynthesis and sun-induced fluorescence at sub-daily to seasonal scales. *Remote Sensing of Environment*, 219, 247–258. <https://doi.org/10.1016/j.rse.2018.10.019>
- van Wittenberghe, S., Alonso, L., Verrelst, J., Moreno, J., & Samson, R. (2015). Bidirectional sun-induced chlorophyll fluorescence emission is influenced by leaf structure and light scattering properties — A bottom-up approach. *Remote Sensing of Environment*, 158, 169–179. <https://doi.org/10.1016/j.rse.2014.11.012>
- Wutzler, T., Lucas-Moffat, A., Migliavacca, M., Knauer, J., Sickel, K., Šigut, L., et al. (2018). Basic and extensible post-processing of eddy covariance flux data with REddyProc. *Biogeosciences*, 15(16), 5015–5030. <https://doi.org/10.5194/bg-15-5015-2018>
- Yang, K., Ryu, Y., Dechant, B., Berry, J. A., Hwang, Y., Jiang, C., et al. (2018). Sun-induced chlorophyll fluorescence is more strongly related to absorbed light than to photosynthesis at half-hourly resolution in a rice paddy. *Remote Sensing of Environment*, 216, 658–673. <https://doi.org/10.1016/J.RSE.2018.07.008>

- Yang, P., & van der Tol, C. (2018). Linking canopy scattering of far-red Sun-induced chlorophyll fluorescence with reflectance. *Remote Sensing of Environment*, *209*, 456–467. <https://doi.org/10.1016/j.rse.2018.02.029>
- Yang, X., Tang, J., Mustard, J. F., Lee, J., Rossini, M., Joiner, J., et al. (2015). Solar-induced chlorophyll fluorescence that correlates with canopy photosynthesis on diurnal and seasonal scales in a temperate deciduous forest. *Geophysical Research Letters*, *42*, 2977–2987. <https://doi.org/10.1002/2015GL063201>
- Zhao, F., Li, R., Verhoef, W., Cogliati, S., Liu, X., Huang, Y., et al. (2018). Reconstruction of the full spectrum of solar-induced chlorophyll fluorescence: Intercomparison study for a novel method. *Remote Sensing of Environment*, *219*, 233–246. <https://doi.org/10.1016/j.rse.2018.10.021>